Crystallographic Analysis of Martensite in 0.2C-2.0Mn-1.5Si-0.6Cr Steel by EBSD

A. J. DeArdo, C. Cayron, L.P. Karjalainen, P.P. Suikkanen

. The crystallography of martensite formed in 0.2C-2.0Mn-1.5Si-0.6Cr steel was studied using the EBSD technique. The results showed that the observed orientation relationship was closer to the Nishiyama-Wassermann (N-W) than to the Kurdjumov-Sachs (K-S) orientation relationship (OR). The microstructure of martensite consisted of parallel laths forming morphological packet-like structures. Typically, there were three different lath orientations in a morphological packet consisting of three specific N-W OR variants sharing the same {111} austenite plane. A packet of martensite laths with common {111} austenite plane was termed as a crystallographic packet. Generally, the crystallographic packet size corresponded to the morphological packet size, but occasionally the morphological packet was found to consist of two or more crystallographic packets. Therefore, the crystallographic packet size appeared to be finer than the morphological packet size. The relative orientation between the variants in crystallographic packets was found to be near 60°/<110>. This appears to explain the strong peak observed near 60° in the grain boundary misorientation distribution. Martensite also contained a high fraction of boundaries with their misorientation in the range 2.5-8°. Typically these boundaries were found to be located inside the martensite laths forming lath-like sub-grains, whose long axes were parallel with the long axis of the martensite laths.

Keywords:
Martensite, austenite, Nishiyama-Wassermann orientation relationship, EBSD, crystallography, packet

INTRODUCTION

Ultra-high strength steels are normally based on martensitic microstructures. Ferrous martensite, in turn, shows a variety of morphologies, such as lath, lenticular or plate, and can be either internally dislocated or twinned for the lattice invariant shear strain , depending on the carbon content. In low-carbon steels (C ~ 0.01-0.2 wt-%), the lath martensite of high dislocation density is the most common morphology and has a paramount industrial significance thanks to an excellent combination of strength and toughness, often in the heat-treated condition [1].

Although martensites have been studied for decades, there still remain unanswered questions. The complete characterization of the type of martensite must include: the type of martensite microstructure and its crystallography, including information such as variant selection and grain boundary misorientations-axis pairs. These details are necessary for a deeper understanding of these structures. Variant selection influences the texture of material and therefore can affect the anisotropy of the physical and mechanical properties of steel [2], whereas the grain boundary misorientations-axis structure can have a major influence on the strength and toughness [3].

The crystallographic analyses of bainite and martensite have been conventionally conducted using X-ray diffraction (XRD). This is a basic and useful method, but has a disadvantage, it does not provide geographical information of microstructure [4]. Another conventional method is transmission electron microscopy, which enables the correlation of accurate crystallographic information to the microstructure. However, the observed areas in TEM are often small (~10μm^2) and analyses of crystallography of larger areas are tedious and are therefore rarely carried out [5].

During the last decade, the electron backscatter diffraction (EBSD) technique has become a popular method in crystallographic studies. EBSD is based on acquisition and analysis of Kikuchi diffraction patterns from the surface of a specimen in a SEM [6]. The diffraction patterns provide crystallographic information that can be related to their position of origin on the specimen. During the last few years, new EBSD data analysis software developments have emerged, among the commercial ones. These softwares, for example, enable more detailed analysis of bainite/martensitic structures [7, 8].

The purpose of the present paper is to study the crystallography of martensite formed in 0.2C-2.0Mn-1.5Si-0.6Cr using the EBSD technique and to analyze these structures by using advanced EBSD software.

MATERIALS AND METHODS

The chemical composition of the investigated steel is given in Table 1. The specimen was cut off from the hot rolled plate and was soaked at 1250 °C for 2 h and water quenched. Cylindrical specimens with a diameter of 6 mm and length of 9 mm were machined from these blanks. These specimens were reheated to

A. J. DeArdo
Department of Mechanical Engineering and Materials Science,
University of Pittsburgh,
636 Benedum Hall, Pittsburgh, PA, 15261-2285, USA,
Tel +1 412-624-9737, Fax +1412-624-9495 – e-mal: deardo@pitt.edu

C. Cayron
CEA, LITEN, 17 rues des Martys, 38054, Grenoble, France

L.P. Karjalainen, P.P. Suikkanen
Department of Mechanical Engineering, University of Oulu,
Box 4200, 90014 University of Oulu, Finland

TAB. 1
The chemical composition of investigated steel in wt-% with calculated martensite start temperature (M_s) and Vickers hardness (HV) for a fully martensitic microstructure.

C	Si	Mn	P	S	Cr	HV (martensite)	Ms, (°C)
0.21	1.48	2.04	0.02	0.006	0.60	477	383

Composizione chimica in peso % degli acciai studiati, con temperatura di inizio trasformazione martensitica calcolata (M_s) e durezza Vickers (HV) per una microstruttura completamente martensitica.

1150°C for 2 min in a Gleeble 1500 thermomechanical simulator, after which they were cooled to room temperature at a rate of 30°C/s to obtain the martensitic structure.
The γ/α' phase transformation start temperature (Ms) was determined on the basis dilatometric curve to be 387 °C. This temperature was found to be in agreement with theoretical martensite start temperature of 383°C calculated on the basis of Equation 1 [9].

$$M_s\,(°C) = 550 - 350C - 40Mn - 20Cr - 10Mo - 17Ni - 8W - 35V - 10Cu + 15Co + 30Al \quad (1)$$

In addition, the measured Vickers hardness (485 HV) matched well with the theoretical hardness for fully martensitic structures (477 HV), as calculated according to Equation 2 [10].

$$HV\,(martensite) = 884C - (1 - 0.3C2) + 294 \quad (2)$$

The specimen was cut in half along the r-h plane of the deformed cylinder, mounted in a conductive mould, then ground and polished according to standard metallographic practices. The final polishing stage was, however, performed using colloidal silica paste (Struers Oxipolish) for 10 min.
The EBSD measurements were carried out in a Zeiss Ultra Plus field emission scanning electron microscope (FE-SEM) equipped with HKL Fast Acquisition software and NordlysF+ EBSD detector. The microscope was operated with an accelerating voltage of 20 kV. The step size for analysis was 0.15 m. The EBSD data analysis was done by HKL Channel 5 software in addition with ARPGE and GenOVa computer program developed at CEA-France. The detailed descriptions of ARPGE and GenOVa programs can found in References [7] and [8], respectively. Retained austenite fractions were determined using Siemens D5000 XRD spectrometer. The austenite fractions were calculated from diffraction data by using Miller's method [11].

RESULTS

General microstructural observations

The microstructure of martensite as observed by EBSD – image quality (IQ) and inverse pole figure (IPF) maps is shown in Figures 1 a and b, respectively. The contrast in the IQ map is related to the brightness of level of diffraction bands above a

FIG. 1
Martensite as seen in EBSD-IQ (a) and IPF (b) maps. White lines in (a) represent the morphological packet boundaries. Grain boundaries with misorientations higher than 15° are coloured black in (b).

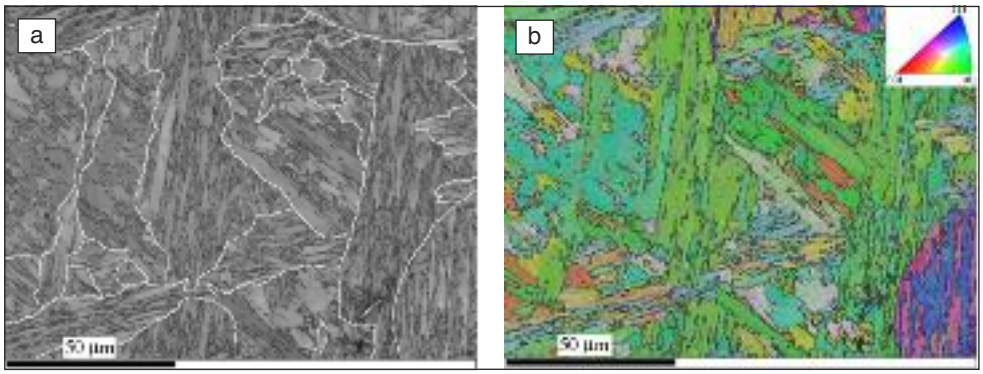

Martensite come vista nelle mappe EBSD-IQ (a) e IPF (b). Le linee bianche in (a) rappresentano i confini dei pacchetti morfologici. I bordi del grano con differenze di orientamento superiori a 15 ° sono di colore nero in (b).

FIG. 2
Experimental <100> (a) and <110> (d) pole figures containing martensite crystal orientations inside a austenite grain. Simulation of theoretical <100> <110> pole figure of the martensite variants inside an austenitic grain assuming K-S OR (b) and (e) and N-W OR (c) and (f).

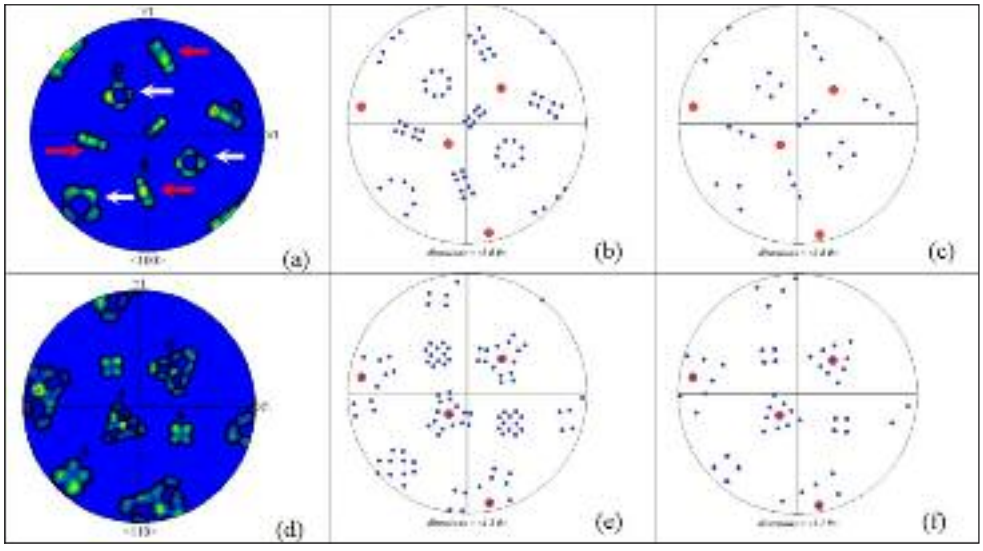

Figure polari sperimentali <100> (a) e <110> (d) contenenti orientamenti dei cristalli di martensite all'interno di un grano di austenite. Simulazione di figura polare teorica <100> <110> delle varianti di martensite entro un grano austenitico assumendo K-S OR [(b) e (e)] e N-W OR [(c) e (f)].

TAB. 2
The 4 most commonly used α/γ orientation relationship models using crystallographic planes and directions.

OR	Plane	Direction
Bain	$\{010\}_\gamma // \{010\}_\alpha$	$<001>_\gamma // <101>_\alpha$
Kurdjumow-Sachs	$\{111\}_\gamma // \{110\}_\alpha$	$<110>_\gamma // <111>_\alpha$
Greninger-Troiano	$\{111\}_\gamma \sim 1° // \{110\}_\alpha$	$<12,17,5>_\gamma // <17,17,7>_\alpha$
Nishiyama-Wassermann	$\{111\}_\gamma // \{110\}_\alpha$	$<011>_\gamma // <001>_\alpha$ or $<112>//<110>$

I 4 modelli di relazione per l'orientamento α/γ più comunemente utilizzati sulla base di piani cristallografici e direzioni.

normalized background, and is affected by the diffraction for a phase, dislocation defect density and grain orientation. Grain boundaries are normally visible as a low image quality (i.e. dark) linear features. The IQ map in Figure 1 a, is a greyscale map and therefore it resembles a SEM image. Figure 1 a shows that martensite consists of groups of parallel or nearly parallel lath-like crystals that form morphological packet-like structures. The morphological packet boundaries are sketched as white boundaries in Figure 1 a. In addition, the uniform greyscale colouring indicates the absence of other γ/α transformation products. The colouring in the IPF map in Figure 1 b shows the crystallographic directions parallel to x-axis of the image, indicated in the stereographic triangle superimposed in the figure. It can be seen from Figure 1 b, that martensite laths are frequently separated by a high angle boundary (i.e., boundaries with their misorientation greater than 15°) as indicated by the black lines. These lath boundaries are thought to be caused by the self-accommodating shear associated with the lath formation.
On the basis of XRD measurements, the retained austenite fraction was below the detection limit of XRD (i.e., below ~ 2%).

Determination of the orientation relationship
There exist four major orientation relationships (OR) to describe the crystallographic correspondence between austenite and martensite in steels: Bain OR [12], Kurdjumov-Sachs (K-S) OR [13], Greninger-Troiano (G-T) OR [14] and Nishiyama-Wassermann (N-W) OR [15]. The parallel crystallographic planes and direction between austenite and phase of aforementioned OR models are listed in Table 2.
Briefly, the Bain OR is simple but very rarely found in nature. Mostly, the K-S and N-W OR are used to describe the experimentally found OR. The G-T OR is an intermediate OR between K-S and N-W OR.
The determination of the OR, without any knowledge of secondary phase, can be realized either by filtering the pole figure [16] or by considering a more complex transformation path, one involving at least two crystal structure-changing micro-mechanism steps[17]. In the present case of martensitic specimen, pole figure filtering (contouring) was applied.
Figures 2 a and d show experimental <100> and <110> pole figures containing martensite crystal orientations inside a single austenite grain. Simulated orientations of martensite crystals (variants) in <100> and <110> pole figures inside a austenite crystal assuming K-S OR are presented in Figures 2 b and e, respectively, and simulated orientations of martensite crystals in <100> and <110> pole figures, assuming N-W OR are shown in Figures 2 c and f, respectively. The simulated pole figures were generated via the GenOVa program [8]. A comparison of the <100> experimental pole figure with the simulated ones reveals that "straight lines" in the experimental pole figure (indicated by red arrows in Figure 2 a) contain 3 intensity maxima, which appear to correspond well with the 3 variants seen in the N-W OR (Figure 2 c). In the K-S OR, these "straight lines" in the <100> pole figure consist of 8 variants (Figure 2 b) and then one could expect to see traces of 8 intensity maxima in the experimental <100> pole figure, also. This is not the case in the present situation. Furthermore, the "squares" with 4 intensity maxima in the experimental <100> pole figure (indicated by white arrows in Figure 2 a) appear to correspond with the 4 variant groups in the simulated <100> pole figure, assuming N-W OR, Figure 2 c. In the K-S OR (Figure 2 b), these sites are occupied by groups of 8 variants forming shapes resembling "circles".
In <110> pole figures, the shapes of "three-fold stars" (seen around the red spots) are revealing: in the K-S OR (Figure 2 e) sides of these "stars" are clearly warped, but in N-W OR (Figure 2 f) the sides are almost straight and form triangles. In the experimental <110> pole figure, the sides of these "three-fold stars" with 10 intensity maxima are clearly straight and match well with the corresponding "three-fold star" consisting of 10 variants in the simulated <110> pole figure assuming the N-W OR (Figure 2 f). In addition, the "squares" with 4 intensity maxima in the experimental <110> pole figure match plausibly with the group of the four variant groups in the simulated <100> pole figure, assuming the N-W OR, Figure 2 f.
On the basis of the qualitative good agreement of experimental and simulated (N-W OR) <100> and <110> pole figures, it was concluded that the OR in the martensitic microstructure is closer to N-W than K-S.

The Nishiyama-Wassermann orientation relationship
As stated in the previous section, the OR in lath martensitic microstructure appears to be closer to N-W than K-S. Therefore, it is interesting to take a closer look at the N-W OR.
A schematic illustration of the three N-W OR crystallographic variants, labeled as variant 1 (V1), variant 2 (V2) and variant 3 (V3), in a common (111) austenite plane with parallel crystallographic directions is presented in Figure 3. The triangle marks

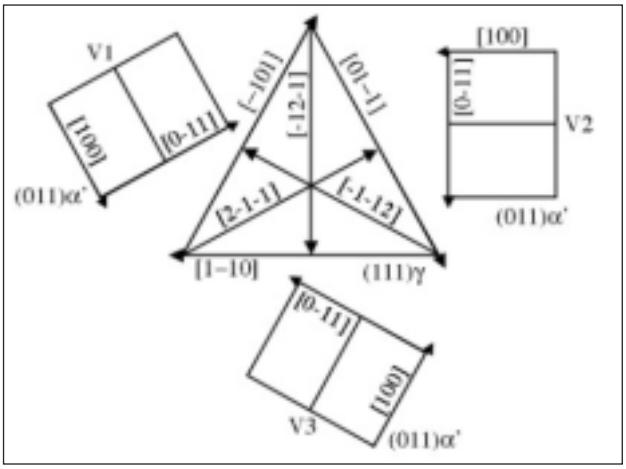

FIG. 3 ***A schematic illustration showing three possible variants formed in (111) austenite plane denoted as variant 1 (V1), variant (V2) and variant 3 (V3).***

Esempio schematico che mostra tre possibili varianti formate in un piano (111) dell' austenite indicate come variante 1 (V1), variante (V2) e variante 3 (V3).

Variant	Crystallographic	Plane parallel	Direction parallel	Direction parallel	Bain Group
V1		$(111)_\gamma$ // $(011)_\alpha$	$[2\text{-}1\text{-}1]_\gamma$ // $[0\text{-}11]_\alpha$	$[1\text{-}10]_\gamma$ // $[001]_\alpha$	A
V2	CP1		$[\text{-}12\text{-}1]_\gamma$ // $[0\text{-}11]_\alpha$	$[\text{-}101]_\gamma$ // $[001]_\alpha$	B
V3			$[\text{-}1\text{-}12]_\gamma$ // $[0\text{-}11]_\alpha$	$[01\text{-}1]_\gamma$ // $[001]_\alpha$	C
V4		$(\text{-}111)_\gamma$ // $(011)_\alpha$	$[\text{-}2\text{-}1\text{-}1]_\gamma$ // $[0\text{-}11]_\alpha$	$[011]_\gamma$ // $[001]_\alpha$	A
V5	CP2		$[12\text{-}1]_\gamma$ // $[0\text{-}11]_\alpha$	$[10\text{-}1]_\gamma$ // $[001]_\alpha$	B
V6			$[1\text{-}12]_\gamma$ // $[0\text{-}11]_\alpha$	$[\text{-}1\text{-}10]_\gamma$ // $[001]_\alpha$	C
V7		$(1\text{-}11)_\gamma$ // $(011)_\alpha$	$[21\text{-}1]_\gamma$ // $[0\text{-}11]_\alpha$	$[110]_\gamma$ // $[001]_\alpha$	A
V8	CP3		$[\text{-}1\text{-}2\text{-}1]_\gamma$ // $[0\text{-}11]_\alpha$	$[0\text{-}11]_\gamma$ // $[001]_\alpha$	B
V9			$[\text{-}112]_\gamma$ // $[0\text{-}11]_\alpha$	$[\text{-}10\text{-}1]_\gamma$ // $[001]_\alpha$	C
V10		$(\text{-}1\text{-}11)_\gamma$ // $(011)_\alpha$	$[\text{-}121]_\gamma$ // $[0\text{-}11]_\alpha$	$[101]_\gamma$ // $[001]_\alpha$	A
V11	CP4		$[\text{-}12\text{-}1]_\gamma$ // $[0\text{-}11]_\alpha$	$[0\text{-}1\text{-}1]_\gamma$ // $[001]_\alpha$	B
V12			$[\text{-}1\text{-}1\text{-}2]_\gamma$ // $[0\text{-}11]_\alpha$	$[0\text{-}1\text{-}1]_\gamma$ // $[001]_\alpha$	C

Tab. 3 The 12 crystallographic variants for N-W OR. *Le 12 varianti cristallografiche per N-W OR.*

represent the (111) austenite plane and the rectangles stand for (011) planes in ferrite. The <112> directions in austenite, which are parallel with <011> directions in martensite, as well as <110> direction in austenite parallel with <100> directions in martensite, are also indicated in Figure 2. Because in the cubic structure, there exist four (111) planes, the total number of variants in N-W OR is 12. These 12 variants, from variant 1 (V1) to variant 12 (V12), are listed in Table 3.

The group of three variants with common {111} austenite or with common {110} ferrite planes can be grouped as so-called crystallographic packets (CP). For a given austenite orientation, there exist four crystallographic packets in N-W OR, as listed as CP1-CP4 in Table 3.

It is also sometimes interesting to group the variants differently. The orientations of 12 N-W OR variants, listed in Table 3, are plotted in a {100} pole figure in Figure 4 a, assuming a (001)[100] orientation for the parent austenite grain. The numbers in this pole figure refer to variant numbers. As seen from Figure 4 a, the variants can be clustered together, like V1, V4, V7 and V10. This clustering derives from the fact that N-W (as well as K-S) correspondence is dominated by the Bain strain, and is, very nearly, a Bain strain followed by rigid body rotation [3]. The orientation of the three Bain OR variants is shown by yellow circles in conjunction with the parent austenite orientation (black dots) in Figure 4 b. The Bain strain is supposed to connect the fcc structure to the bcc structure via a tetragonal intermediate strain, and is characterized by axis compression, which may lie along any of the three cubic axes of the fcc. However, it has recently been shown that the Bain model is not in agreement with the EBSD pole figures, and an alternative model of martensitic transformation has been proposed [18].

There are three distinct so-called Bain variant groups or packets, which can be identified in a {100} pole figure, as indicated by different colors in Figure 4 b. If the compression along the y-axis is labelled Bain variant A, with B for the x-axis and C for the z-axis, then the N-W OR variants can be separated into Bain groups. By comparing Figure 4 a and b, it can be seen that Variants 1, 4, 7 and 10 belong to a Group A (red circles), variants 2, 5, 8 and 11 comprise the Bain Group B (black circles) and variants number 3, 6, 9 and 12 belong to the Bain group C (blue circles). The Bain groups are also listed, Table 3. As seen from Figure 4 b, crystals belonging in same Bain variant group have nearly parallel {100} ferrite planes, although in N-W (or K-S) OR they are never exactly parallel.

On the basis of the metallographic results in the section "General microstrctural observations" and the definition of N-W OR in the previoussection, it was decided to define three different "packets". The definitions of these packets are as follows:

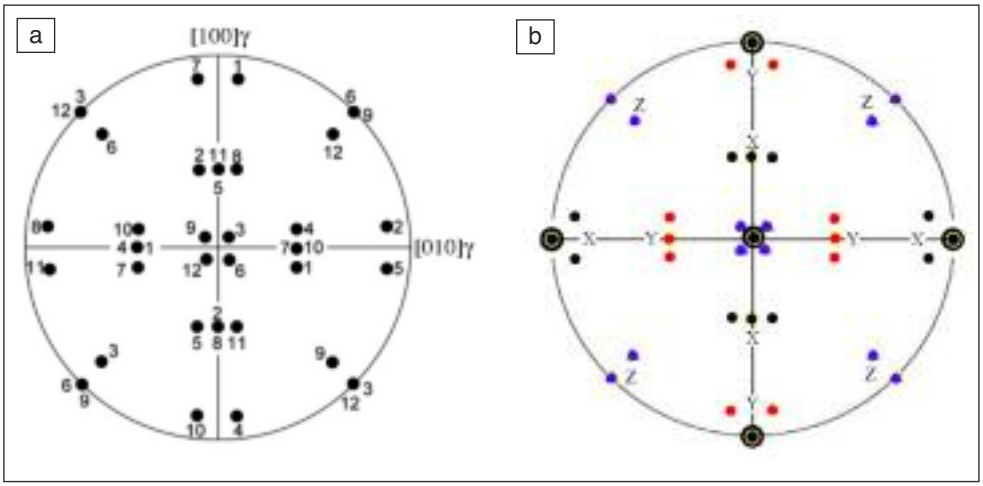

FIG. 4
The pole figure showing the orientations of the 12 martensite variants transformed from (001)[100] oriented austenite keeping the N-W OR. The number indicates the variants of martensite (a). Stereographic projection of N-W variants (full symbols) showing that the various N-W OR variants are clustered together according to Bain group (b). The yellow symbols indicate the orientation of Bain variants.

Figura polare che mostra gli orientamenti delle 12 varianti di martensite trasformata da austenite orientata (001) [100] assumendo la N-W OR. Il numero indica le varianti di martensite; (a). Proiezione stereografica per le varianti N-W (simboli pieni), che mostra che le diverse varianti N-W OR sono raggruppate secondo il gruppo di Bain (b). I simboli in giallo indicano l'orientamento delle varianti di Bain.

I. Morphological packet is a group of parallel or nearly parallel lath-like crystals. An example of morphological packets is seen Figure 1 a.
II. Crystallographic packet is a group of lath crystals with common {110} martensite planes (or equivalently {111} austenite planes). The four crystallographic packets in N-W OR are numbered in Table 3 as CP1-CP4. There exist 3 variants in each crystallographic packet as a maximum.
III. Bain packet (or group) is a group of crystals planes oriented around the Bain relation as, shown in Figure 4 b. (i.e., these crystals have nearly common (100) plane).

The relative orientation between N-W OR variants

The general calculations of the variants and specific misorientations between them can be described algebraically by cosets and by double-cosets, respectively. The calculations are automatically performed with dedicated software called GenOVa [8]. For a better understanding, we prefer here to give the details of the manual calculations. The misorientation angle-axis pairs between the N-W OR variants can be determined as follows:

The change in crystallographic orientation through the γ/α phase transformation is expressed by a matrix equation:

$$M = TA \quad (3)$$

where M and A are the orientation matrices for martensite and austenite, respectively and T is a orientation transformation matrix for N-W. There exist 12 orientation transformation matrices for the N-W OR and these matrices (T_1-T_{12}) are listed, for example, in Reference [5]. For a given austenite orientation, application of Equation 5 with 12 transformation orientation matrices, leads to generation of 12 orientation matrices for martensite (M_1-M_{12}). On the basis of these orientation matrices, the ideal orientation for martensite crystals can be extracted. Assuming an orientation of (001)[100] for parent austenite in the recrystallized condition, the 12 possible orientations for martensite crystals are listed in Table 4.

The relative orientation between two variants can be determined on the basis of the rotation matrix, R:

$$R = M_x M_y^{-1} \quad (4)$$

where M_x and M_y are the orientation matrices for x^{th} and y^{th} variant for martensite.

The rotation matrix R can be expressed in the form:

$$R = \begin{Bmatrix} a_{11} & a_{12} & a_{13} \\ a_{21} & a_{22} & a_{23} \\ a_{31} & a_{32} & a_{33} \end{Bmatrix} \quad (5)$$

where a_{ij} are column vectors of direction cosines between Cartesian axes.

In cubic material, because of symmetry, the relative orientation of two variants can be described in 24 ways. These orientations can be found by multiplying the rotation matrix with 24 so-called symmetry matrices C_i (i = 1-24):

$$C_i R \quad (6)$$

The symmetry matrix C is a 3 x 3 matrix composed of three elements equal to +1 or -1 and six elements equal to 0. Symmetry matrices, can be found (for instance) in Reference [19].

The rotation angle can be extracted from the rotation matrix R by [5]:

$$\cos\theta = (a_{11}+a_{22}+a_{33}-1)/2 \quad (7)$$

The direction of rotation axis r ($<r_1, r_2, r_3>$) can be calculated from rotation matrix R [19]:

$$\begin{aligned} r_1^2 &= (a_{11}-\cos\theta)/(1-\cos\theta), \\ r_2^2 &= (a_{22}-\cos\theta)/(1-\cos\theta), \\ r_3^2 &= (a_{33}-\cos\theta)/(1-\cos\theta) \end{aligned} \quad (8)$$

As mentioned above, there are 24 combinations of rotation matrices, which in turn lead to the different misorientation angle-pairs (even thought they all describe the same relative orientation). The rotation matrix, which gives the lowest misorientation angle, also called disorientation, is taken as the answer.

Setting V1 as the reference variant, the relative orientation (misorientation angle-axis pair) of other variants with respect to V1 can be then calculated using the procedure described above. The relative orientations of V2-V12 with respect to V1 are represented in Table 5. By repeating this procedure setting other variants (V2-V12) as the reference variant, it is possible to find all variant pairs corresponding to certain misorientation angle-axis pairs. These pairs are listed in Table 5.

According to Table 5, there exist five possible misorientation

Variant	Orientation (hkl)[uvw]	Relative orientation in respect to Variant 1	
		Misorientation angle,°	Misorientation axis
V1	(-0.71 0.70 0.12) [0.00 -0.17 0.99]	-	[-]
V2	(-0.71 0.12 0.70) [0.71 -0.12 0.70]	60.0	[0.00 -0.71 -0.71]
V3	(0.00 0.99 -0.17) [-0.71 0.12 0.70]	60.0	[0.00 0.71 0.71]
V4	(-0.71 0.99 -0.17) [-0.00 0.169 0.99]	19.5	[1.00 0.00 0.00]
V5	(-0.70 0.12 0.71) [0.70 -0.12 0.71]	53.7	[-0.22 -0.70 0.68]
V6	(-0.17 0.99 0.00) [-0.70 -0.12 0.70]	53.7	[-0.22 0.70 0.68]
V7	(-0.70 0.71 0.12) [0.17 0.00 0.99]	13.7	[0.71 -0.71 -0.06]
V8	(-0.12 0.71 .070) [-0.12 -0.71 0.70]	53.7	[0.68 -0.22 0.70]
V9	(-0.99 0.17 0.00) [-0.12 -0.70 0.71]	50.0	[-0.62 0.47 -0.62]
V10	(-0.12 0.70 0.71) [-0.17 0.00 0.99]	13.7	[0.71 0.71 0.06]
V11	(-0.12 0.70 0.71) [0.12 -0.70 0.71]	50.0	[-0.62 0.47 0.62]
V12	(-0.99 0.00 0.17) [0.12 -0.71 0.70]	53.7	[-0.68 0.22 0.70]

TAB. 4 ***Crystal orientation of martensite variants transformed from (001)[100] austenite and relative orientation between V1 and other variants.***

Orientamento dei cristalli di varianti di martensite trasformata da austenite (001) [100] e orientazione relativa tra V1 e altre varianti.

Op	Misorientation	Axis	Axis (low-index Miller indices)	Between variants* (*Note that for example V1-V2 ó V2-V1)
O_1	60.00°	<0.00 0.71 0.71>	<011>	V1-V2, V1-V3, V2-V3, V4-V5, V4-V6, V4-V5 V7-V8, V7-V9, V8-V9, V10-V11, V10-V12, V11-V12
O_2	53.7°	<0.22 0.70 0.68>	<133>	V1-V5, V1-V6, V1-V8, V1-V12, V2-V4, V2-V7, V2- V9, V2-V12, V3-V4, V3-V8, V3-V10, V3-V11, V4-V9, V4-V11, V5-V9, V5-V10, V5-V12, V6-V7, V6-V8 V6-V11, V7-V11,V7-V12, V8-10, V9-V10
O_3	50.0°	<0.63 0.47 0.63>	<434>	V1-V9, V1-V11, V2-V6, V2-V10, V3-V5, V3-V7, V4-V8, V4-V12, V5-V7, V6-V10, V8-V12, V9-V11
O_4	19.5°	<1.00 0.00 0.00>	<100>	V1-V4, V2-V8, V3-12, V5-V11, V6-V9, V7-V10
O_5	13.8°	<0.06 0.68 0.70>	<011>	V1-V7, V1-10, V2-V5, V2-V11, V3-V6, V3-V9, V4-V7, V4-V10, V5-V8, V6-12, V8-V11, V9-V12

TAB. 5 ***Calculated misorientation angle-axis pairs between martensite variants in N-W OR and the variant pairs that comprise the particular angle-axis pairs. Note: Operator O_2 is a polar operator (the set of equivalent rotations from Vi to Vj, which is the set of the inverses of the equivalent rotations from Vj to Vi, is different from the set of the equivalent rotations from Vj to Vi.***

Coppie di disorientamento angolo-asse calcolate tra varianti di martensite in N-W OR e le coppie di varianti che costituiscono le particolari coppie angolo-asse. Nota: l'operatore O_2 è un operatore polare (l'insieme delle rotazioni equivalenti da Vj a Vi, che è l'insieme degli inversi delle rotazioni equivalenti da Vj a Vi, è diverso dalla serie delle rotazioni equivalenti da Vj a Vi.

angle-axis pairs between the variants in N-W OR. The specific misorientations between the variants are called operators (O_1-O_5). The operator with the highest misorientation (60.0°/<011>) is O_1. This operator is only possible when variants share the same {111} austenite plane (i.e. between variants V1-V3, V4-V6, V7-10 and V10-12). The other operators with high misorientations are O_2 (53.7°/<133>) and O_3 (50.0°/<434>). These operators are possible between the variants with different {111} austenite plane. The operators with lowest theoretical misorientations O_4 (19.5°/<001>) and O_5 (13.8°/<011>) are observed between variants 1, 4, 7 and 10, between variants 2, 5, 8 and 11 and 3, 6, 9 and 12. These groups correspond to Bain groups A, B and C, respectively, as listed in Table 5.

Identifying the N-W OR variants and the crystallography of martensite

The identification of N-W OR variants on the basis of EBSD data was performed as follows: Figure 5 a showed a simulated {100} pole figure containing the positions of 12 N-W OR variants for martensite transformed from a (001)[100] oriented austenite. The variant numbering in this pole figure was based on variant numbering in Table 3. An experimental {100} pole figure containing martensite crystal orientations inside a single austenite grain was shown in Figure 4 a. The experimental pole figure was rotated in such a way that it coincides with the simulated pole figure (transformed from a (001) [100] oriented austenite). Figure 5 shows the simulated {100} pole figure (Figure 4 a) superimposed on the (rotated) experimental {100} pole figure. It is seen from Figure 5 that all twelve variants are easily identifiable, and then by using EBSD mapping software, one can identify the N-W OR variants in the martensitic microstructures in inverse pole figure or Euler angles maps. The identification of the variants can also be performed automatically with a dedicated software called ARPGE [7].

The results showed that martensite consists of parallel (or nearly parallel) lath-shaped crystals which form morphological packets. Typically, the morphological packets consist of a group of parallel laths which have three different orientations. The three orientations of laths in the morphological packets consist of three specific N-W OR variants sharing the same {111} austenite plane, such as V4, V5 and V6. An example of this is illustrated in Figure 6, which shows two morphological packets in martensite: Variants V4, V5 and V6 comprise one morphological packet and variants V10, V11 and V12 constitute another one. As defined in section "The Nishiyama-Wassermann orientation relationship", when the martensite crystals share the common {111} austenite (or common {110} ferrite planes), the formed group can be called a crystallographic packet. In many cases, crystallographic packets were found to correspond to the morphological packets. However, in some cases, it was found that the crystallographic packet size and morphological packet size did not agree. This is illustrated in Figure 7, where crystallographic packets are differentiated by different colours using the ARPGE program. If applying the same labelling as in Table 3, the red, green, yellow and blue packets correspond CP1, CP2, CP3 and CP4, respectively. It is seen from Figure 7 that occasionally a morphological packet consist two or more crystallographic packets. For example, the approximate minimum dimension of the morphological packets shown in Figure 6 are larger than approximately 20-30 μm, whereas the crystallographic packets shown by the ARPGE progran in Figure 7 are of the approximate minimim dimension of 10-20 μm. Therefore, the crystallographic packet size appears to be finer, at least in some cases, than the morphological packet size. It was shown in Table 5 that the relative orientation between two adjacent N-W OR variants with a common {111} plane is always 60°/<110> (i.e. O1) and this was confirmed to hold true experimentally for some of the adjacent variants too. On the other hand, the most typical misorientation angle-axis pair between the neighboring laths in a morphological packet was 59.8°/<343>, Figure 8 a and b. However, it should be noted that 59.8°/<343> is only ~ 1° away from the operator O_1 = 60° /<110>, since this operator is also equals to 60.8°/ <343> (in the set of equivalent rotations).

It is also notable that the lath-martensite contained a high fraction of boundaries with their misorientations in the range of 2.5 - 8°. This is clearly detected in Figure 8 a, which shows that there exists a strong peak at ~ 3.5° in the grain boundary misorientation (GBM) distribution. The rotation axis of these low-

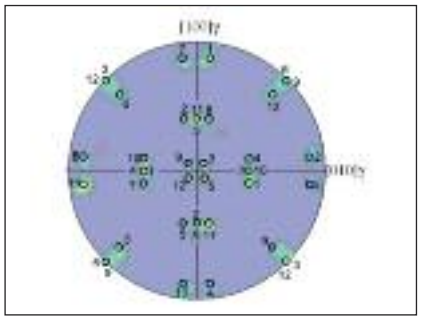

FIG. 5
The contoured {100} pole figure containing orientations inside a single austenite grain for martensitic specimen. The theoretical {100} pole figure with N-W OR variants labelled (V1-V12) transformed (001)[100] oriented austenite is superimposed on the experimental pole figure.

La figura polare {100} contenente le orientazioni all'interno di un singolo grano di austenite per provino martensitico. La figura polare terica {100} con varianti N-W OR contrassegnate (V1-V12) austenite orientata trasformata (001) [100] è sovrapposta alla figura polare sperimentale.

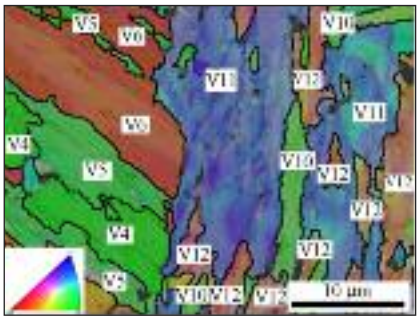

FIG. 6
Inverse pole figure maps of martensite laths in two crystallographic packets. The identified variant numbers are also shown in the figure.

Mappe della figura polare inversa di aghi di martensite in due pacchetti cristallografici. Sono anche mostrati in figura i numeri varianti identificati.

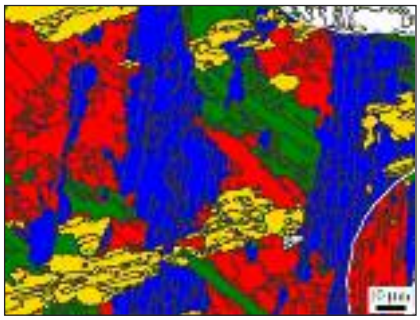

FIG. 7
Crystallographic packets (CP) in martensite. Using the labelling given in Table 3, red, green, yellow and blue packets correspond to CP1 (i.e. common [111] austenite plane), CP2 (common [-111] austenite plane), CP3 (common [1-1 1] austenite planes) and CP4 (common [-1-11] austenite plane), respectively.

Pacchetti cristallografici (CP) nella martensite. Utilizzando i contrassegni di Tabella 3, i pacchetti rossi, verdi, gialli e blu corrispondono rispettivamente a CP1 (piano di austenite comune [111]), CP2 (piano di austenite comune [-111]), CP3 (piano di austenite comune [1-1 1]) e CP4 (piano di austenite comune [-1-11]).

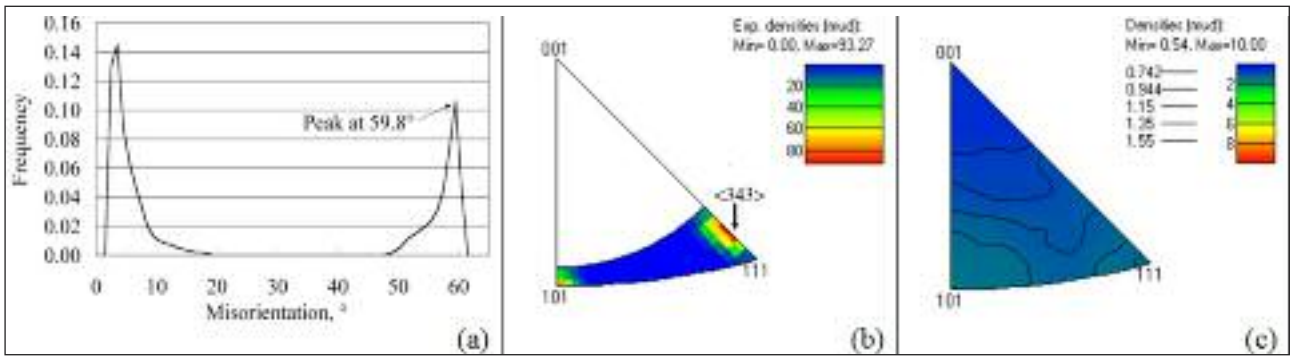

Fig. 8 Grain boundary misorientation (GBM) distributions for martensite (b). Rotation axes in crystal coordinate system for the boundaries with their misorientations from 58° to 62 (b). Rotation axis in crystal coordinate system for the boundaries with their misorientations in the range of 2.5-8° (c).

Distribuzione del disorientamento dei bordi del grano (GBM) per la martensite (b). Asse di rotazione nel sistema di coordinate dei cristalli per i bordi con disorientamento compreso tra 58 ° e 62 (b). Asse di rotazione nel sistema di coordinate dei cristalli per i bordi con disorientamento nel campo tra 2,5 e 8 ° (c).

angle boundaries was found to be randomly distributed, even thought there existed a weak trend for the rotation axis to be concentrated towards <110>, as shown in Figure 8 c. The continuous small rotation around <110> is in agreement with the second step of the 2-step model proposed earlier [18], as will be discussed later. Boundaries with their misorientation in the range of 2.5-8° were typically found to be located inside the martensite laths. They clearly formed lath-like sub-grains, whose long axes are parallel with the long axis of martensite as seen in Figure 9.

Grain boundaries with their misorientation in the range of 10 - 20° or 49 - 55° were not frequently observed in this martensitic structure, as seen from the GBM distribution in Figure 8 a, although N-W OR is able to produce misorientations in the aforementioned ranges, if operators O_5 (13.8° / <011>), O_4 (19.5° / <001>), O_3 (50°/<434>) and O_2 (53.7°/<133>) exists, as seen from Table 5. When grain boundaries in the range of 10 - 20° or 49 - 55° were observed in the microstructure, they were typically located at the sites where two crystallographic packets adjoin. An example of this is presented in Figure 10, which shows a boundary between two crystallographic packets. (One crystallographic packet consists of variants V7, V8 and V9 and second one is made of variants V1 and V3). The grain boundaries with their misorientation in the range 9 - 16° and 49 - 55° are coloured as red and white lines, respectively. The other high-angle boundaries are marked as black lines. It is clearly seen that a low-angle boundary (θ= 9 - 16°) is always observed between variants V3 and V9, but there exists a high-angle boundary (θ= 49

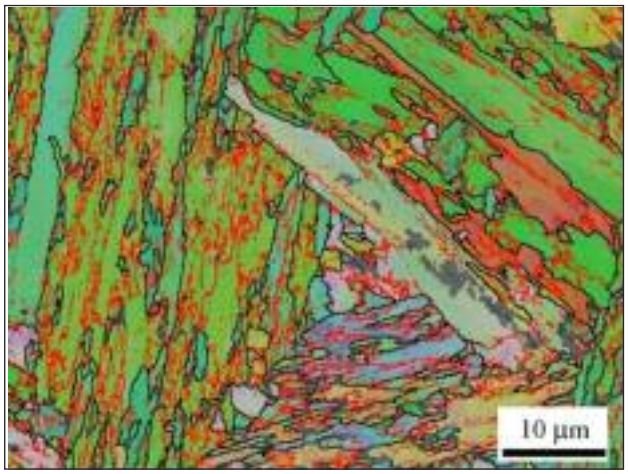

FIG. 9 ***Grain boundaries with their misorientation in the range 2.5-8° coloured red in the martensite.***

Bordi di grano con disorientamento nel campo di 2,5-8 ° colorato in rosso nella martensite.

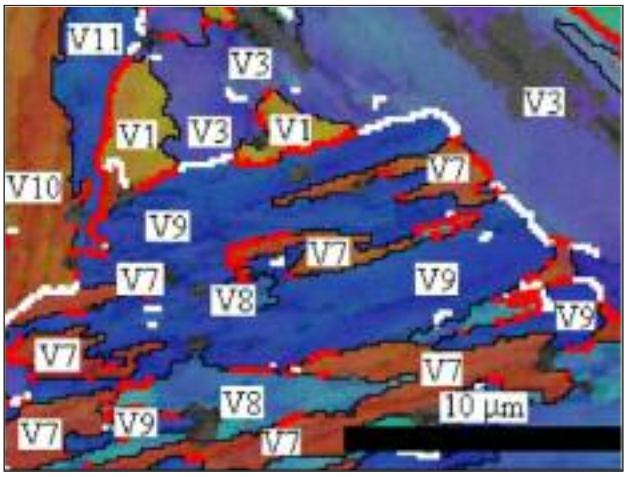

FIG. 10 ***Inverse pole figure map showing the boundary between two crystallographic packets. The boundaries with misorientation in the range of 17-21° and 49-54° are coloured as white and red lines, respectively. Other high-angle grain boundaries are marked black.***

Mappa della figura polare inversa che mostra il bordo tra due pacchetti cristallografici. I bordi con disorientamento nel campo tra 17-21 ° e 49-54 ° sono segnati rispettivamente con linee bianche e rosse. Altri bordi di grano ad alto angolo sono segnati in nero.

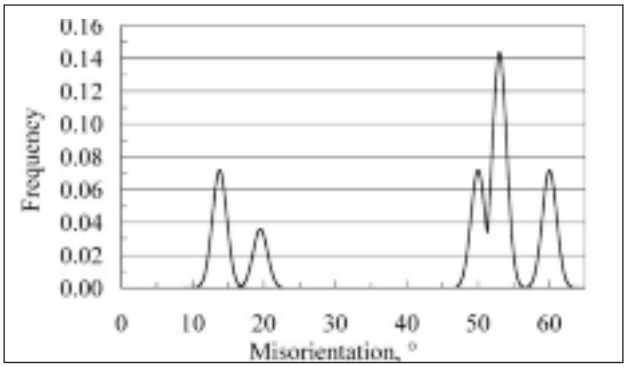

FIG. 11 ***Theoretical misorientation angle distribution for N-W OR variants formed in same austenite grain. All variant pairs are assumed to have the same probability to form.***

Distribuzione teorica del disorientamento dell'angolo per varianti N-W OR formate nello stesso grano di austenite. Tutte le coppie di varianti si assume abbiano la stessa probabilità di formarsi.

- 55°) between V1 and V9 or between variants V3 and V7. Theoretical calculations given in Table 5, show that the operator between variants V3-V9 is O_5 (13.8°/<011>), whereas the operator between variants V1 and V9 or between variants V3 and V7 is O_3 (50.0°/<434>).
A comparison of Tables 3 and 5 shows that operators O_4 and O_5 are formed between variants belonging to same Bain group or packet, but different crystallographic packets, whereas operator O_3 and O_2 are formed between variants belonging to different crystallographic packets and also to different Bain groups.

DISCUSSION

The OR relationship between austenite and martensite in low C steels with lath martensitic structures has been studied extensively during the last decades mainly using TEM. The results are not fully consistent. Typically, the OR has been found to be near K-S OR [20, 21, 22, 23], but other studies have found ORs near N-W OR [24], mixed K-S and N-W [25, 26] or near G-T OR [27, 28]. The qualitative result in the present work, based on the comparison of experimental and simulated pole figures, clearly shows that the operative OR in lath-martensite formed in 0.2-2.0Mn-1.5Si-0.6Cr steel is closer to N-W OR than K-S OR, although a detailed analysis of deviation from the exact N-W OR was not performed here. However, the identification of variants successfully located all N-W OR variants in the microstructure and no clear signs of variants falling outside the N-W OR were found, indicating the validity of the concept and method.
It is highly evident that strong local variant selection takes place during the martensitic transformation. This is easily detected, when comparing the experimentally determined GBM distribution in Figure 8 a with the theoretical one shown in Figure 11. In Figure 11, it is assumed that all NW OR variant pairs have the same probability to form as their fraction of occurrence. It is clearly seen that experimentally determined GBM distributions differ considerably from theoretical ones. This discrepancy derives from the variant selection. It was shown in Figure 6 that martensite consisted typically of groups of parallel lath-like crystals, whose orientation was dictated by two or three specific N-W OR variants sharing the same {111} austenite plane. Furthermore, it was shown in Table 5 that the relative orientation between two adjacent variants with common {111} is always 60°/<110>. Experimentally, the relative orientation between adjacent variants in a crystallographic packet was found to be near 60°/<110>. The variant selection thereby explains the strong peaks around 60° in GBM distribution in Figure 8 a.
On the basis of the theoretical GBM distribution in Figure 11, one could also expect to see pronounced peaks in the experimental GBM distribution in the ranges of 10-20° and 45-55°, due to formation of operators of O_2-O_5. However, in the experimental GBM distribution no clear peaks in the aforementioned ranges were observed, Figure 8 a. This can be explained by the fact that grain boundaries with their misorientations were mainly found between variants that belong to different crystallographic packets and were located at the sites where two crystallographic packets unite. Since the grain boundary length

between variants inside the crystallographic packets appears to be much higher than the grain boundary length between different crystallographic packets, it is natural that strong peaks arise near 60° in the experimental GBM distribution, but the existence of peaks near 10 - 20° and 45 - 55° is suppressed.

Variant selection is generally (in the absence of retained deformation) explained by the tendency of steels to accommodate plastic strains induced in austenite during transformation, and thereby to enhance martensite transformation. For example, in the case of high C martensite, it is well-known that martensite plates usually have specific combination of variants in order to accommodate the transformation strains [29]. In the present case, it is notable that three different variants were generally observed in a crystallographic packet and there was no strong tendency for certain variants to form couples within the crystallographic packet. It has been reported that in martensite in a Fe-28Ni alloy [5] and in isothermally transformed bainitic 0.79C-1.5Si-0.98Cr- 0.24Mo-1.06Al-1.58Co steel [30], both apparently obeying N-W OR, that specific combinations of two NW-OR variants with common {111} austenite planes appeared in limited areas.

Since the lowest misorientation produced by N-W OR between two adjacent variants is 13.5° about <110> (O_5), Table 5, the formation of low-angle boundaries in the range of 2 - 8° in martensite (Figure 8 a) with randomly distributed rotation axis (although there existed a weak tendency of rotation axis to be clustered around <110> axis), cannot be directly linked to the crystallography nature of martensite transformation (i.e. deriving from the N-W OR). However, based on the EBSD measurements, the existence of this type of low-angle boundary structure is often reported in the literature. For example, Sonderegger et al. [31] found that the rotation axis of the low-angle boundaries in 0.17C - high Cr (9-12%) creep-resistant steel in the martensitic condition were completely random and no favored misorientation was observed. A similar observation of widely dispersed rotation axes was also made in high C martensitic ball bearing steel tempered at 160°C in the paper by Ryde [32]. In addition, TEM results by Morito et al. [23] showed that there exist large variations in the nature of low-angle grain boundaries in lath martensite formed in an IF-steel, ranging from near tilt to near pure twist boundaries.

There indeed appears to exist a certain degree of orientation spread within the martensite laths. This is observed not only by the presence of low-angle boundary structure (Figure 9) but also as the gradation of colors in IPF maps (Figure 6 and Figure 10). In addition, the experimental pole figure reveals that there is an observable spread in martensite. For example, Figure 12 shows the same experimental <110> pole figure for martensitic crystal orientation inside a single austenite grain as presented in Figure 2 d. The difference is that Figure 12 does not contain data convolution (contouring) like Figure 2 d does, but represents the experimental data with inverse pole figure map coloring. The <110> pole figure of the martensitic crystal orientation in Figure 12 does not show sharp dots (i.e., intensity maxima) as could be expected with well-defined variant orientations. In fact, it shows continuous lines forming singular features. Similar features appear in many fcc–bcc martensitic materials such as CuZn brasses, bainitic steels and FeNi meteorites as summarized in Reference [18]. They are not artifacts that could be attributed to the EBSD method, as Bunge et al. [33] also observed them by synchrotron X-ray diffraction. One could speculate that these features could be simply explained by the plasticity of parent austenite. However, a new theory proposed by Cayron et al. [18] suggests that the singular (continuous) features in pole figures correspond to a trace or sequence of the transformation micro-

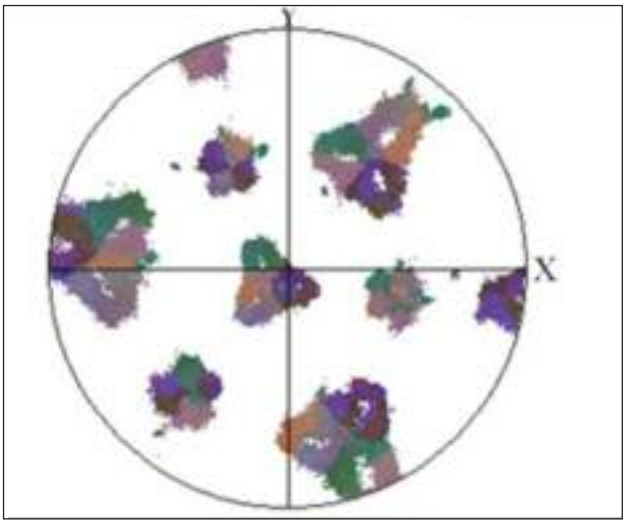

FIG. 12 ***An experimental <110> pole figure containing martensite crystals orientated within a single austenite grain.***

Figura polare sperimentale <110> contenente l'orientamento dei cristalli di martensite all'interno di singoli grani di austenite.

mechanisms. In this theory, the fcc–bcc transformation is not a single step reaction or a deformation implying Bain distortions, but results from a fcc–hexagonal close-packed (hcp) step followed by an hcp–bcc step. The continuous features in the experimental EBSD as well as X-ray pole figures of fcc–bcc martensitic materials can be simulated by two continuous rotations: one around [1 1 0] austenite of angles varying between 0° and 10° and one around [1 1 1] austenite (= [110] martensite) of angle varying between 0° and 5°. Our observations of the internal deformations of a few degrees with a tendency around the <110> martensite axes is in agreement with the last step of the model.

Conclusions

Crystallography of lath-martensite in 0.2C-2.0Mn-1.5Si-0.6Cr steel was investigated using EBSD technique. The major results are summarized as follows:

1. The orientation relationship between austenite and martensite is closer to Nishiyama-Wassermann (N-W) than Kurdjumov-Sachs orientation relationship.
2. The microstructure consists of parallel or nearly parallel laths forming a packet-like structure. There are typically three different orientations in a packet. The three orientations of laths in the packet correspond to three specific N-W OR variants sharing the same {111} austenite plane or consequently variants have a common {110} martensite plane. This type of packet is then termed a crystallographic packet.
3. Generally, the crystallographic packet size corresponded to the morphological packet size, but occasionally the morphological packet was found to consist of two or more crystallographic packets. Therefore, the crystallographic packet size appears to be finer than the morphological packet size.
4. The relative orientation between the variants with a common {111} austenite plane was found to be near 60°/<110>. This explains the strong peaks at 60° in the grain boundary misorientation distribution.
5. Martensite contains a high amount of low-angle boundaries (i.e., sub-grain boundaries) with their misorientation in the range 2.5-8° (i.e., sub-grain boundaries). The rotation axis of these boundaries was found to be widely dispersed, although there is a weak tendency for these axes to be clustered

around <110>. Typically these boundaries were found to be located inside the martensite laths forming lath-like subgrains, whose long axes are parallel with the long axis of martensite laths.

6. The misorientation and angles (i.e., 13.8°/<110>, 19.5°/<100>, 50.0°/<434 > and 53.7°/<331>) that can be produced by N-W OR were not frequently found in the structure, but, when observed, they were observed typically between the boundaries of two different crystallographic packets.

ACKNOWLEDGEMENT

Funding of The Finnish Funding Agency for Technology and Innovation (Tekes) is gratefully acknowledged in the project QaMiS (DNo 1691/31/07; No 40197/07).

REFERENCES

[1] G. Krauss: STEELS - Heat treatment and processing principles, Metals Park, Ohio ASM International, 1990.
[2] R.K. Ray and J.J. Jonas: Int. Mat. Rev. 1990 35 ,1 1.
[3] Z. Guo, C.S. Lee, J.W. and Morris Jr.: Acta Mater., 2004, 52, 55.
[4] Z. Nishiyama: Martensitic Transformation, New York, Academic Press, , 1978.
[5] H. Kitahara, R. Ueji, M. Ueda, N. Tsuji and Y. Minamino: Mater. Charact., 2005, 54, 378.
[6] V. Randle: Mater. Charact., 2009, 60 913.
[7] C. Cayron: J. Appl. Crystallogr., 2007, 40, 1183.
[8] C. Cayron: J. Appl. Crystallogr., 2007, 40, 1179.
[9] W. Steven and A.G. Haynes, J. Iron Steel Inst., 1956, 183, 349.
[10] N. Yurioka, M. Okumura, T. Kasuya, and H. Cotton, Metal Constr., 1987, 19, 217.
[11] R.L. Miller: Trans. ASM, 1964, 57, 892.
[12] E.C. Bain: Trans. AIME Steel Division, 1924, 79, 25.
[13] G. V. Kurdjumov and G. Sachs: Z. Phys., 1930, 64, (1930) 325.
[14] A.B. Greninger, and A.R. Troiano: J. Met. Trans., 1949, 185, 590.
[15] Z. Nishiyama: Sci. Rep. Tohoku Imp. Univ., 1934 23, 637.
[16] G. Nolze and V. Geist: Cryst. Res. Technol., 2004, 39, 343.
[17] G. Miyamoto, N Takayama and T. Furuhara: Scr. Mater., 1990, 60, 1113.
[18] C. Cayron, F. Barcelo and Y. de Carlan: Acta Mater., 2010, 58, 1395.
[19] V. Randle and O. Engler: Introduction to Texture Analysis: Macrotexture and Orientation Mapping, Amsterdam, Gordon and Breach Science Publishers, 2000.
[20] K.Wakasa and C.M. Wayman; Acta Metall., 1981, 29, 991.
[21] J.M Chilton, C.J. Barton and G.R. Speich: J. Iron Steel Inst., 1970, 208, 184.
[22] H. Kitahara, R. Ueji, N. Tsuji and Y. Minamino: Acta Mater., 2006 54, 1279.
[23] S. Morito, X. Huang, T. Furuhara, T. Maki, and N. Hansen: Acta Mater., 2006, 54, 5323.
[24] D.S. Sarma, J.A Whiteman, J.H. Woodhead: Met. Sci., 1976, 10, 391.
[25] B.V.N. Rao and G. Thomas: ICOMAT 1979, Proc. Int. Conf. on Martensitic Transformations; Cambridge; Massachusetts, USA, 1979, 12.
[26] B.V.N. Rao: Metall. Trans. A, 1978 10, 645.
[27] B.P.J. Sandvik and C.M. Wayman:, Met. Trans. A, 1983, 14A, 809.
[28] C.P Luo and J. Liu:, Mater. Sci. Eng. A, 2006, 438-440, 149.
[29] H. Okamoto, M. Oka and I. Tamura: Trans. JIM, 1978, 19, 674.
[30] H. Beladi, Y. Adachi, I. Timokhina and P.D. Hodgson:, Scr. Mater., 2009, 60, 455.
[31] B. Sonderegger, S Mitche and H. Cerjak:, Mater. Charact.,2007, 58, 874.
[32] L. Ryde: Mater. Sci. Techn., 2006, 22, 1297.
[33] H.J. Bunge, L. Wcislak, H. Klein, U. Garbe and J.R. Schneider: Mat. Sci. For., 2002, 408- 412, 137

Abstract

Analisi Cristallografica della Martensite in un acciaio 0.2C-2.0Mn-1.5Si-0.6Cr mediante EBSD

Parole chiave: acciaio, cristallografia

Nel presente lavoro è stata studiata la cristallografia della martensite formata in un acciaio 0.2C-2.0Mn-1.5Si-0.6Cr mediante tecnica EBSD (electron backscatter diffraction). I risultati hanno mostrato che la relazione di orientamento osservata (OR). è più vicino a quella di Nishiyama-Wassermann (NW) piuttosto che a quella di Kurdjumov-Sachs (KS). La microstruttura della martensite era caratterizzata da aghi paralleli che formavano strutture morfologiche a pacchetto. In genere, si sono evidenziati tre diversi orientamenti degli aghi in un pacchetto morfologico costituito da tre varianti specifiche del N-W OR, che avevano in comune lo stesso piano {111} dell' austenite. Un pacchetto di aghi di martensite che avesse lo stesso piano {111} dell' austenite è stato definito come un pacchetto cristallografico. In generale, la dimensione del pacchetto cristallografico corrispondeva a quella del pacchetto morfologico, anche se talvolta il pacchetto morfologico è risultato essere composto da due o più dei pacchetti cristallografici. Pertanto, la dimensione del pacchetto cristallografico appariva più fine rispetto alla dimensione del pacchetto morfologico. L'orientamento relativo tra le varianti nei pacchetti cristallografici è risultato essere vicino a 60° / <110>. Ciò sembra spiegare il forte picco osservato vicino a 60° nella distribuzione del disorientamento del bordo del grano. Anche la martensite conteneva una percentuale elevata di bordi con differenze di orientamento fra 2,5 e 8°. Tipicamente questi bordi sono stati localizzati entro gli aghi di martensite formandovi pseudo sottograni, il cui asse longitudinale risulta parallelo all' asse longitudinale degli aghi di martensite.